Supplement of Atmos. Chem. Phys., 26, 5713–5725, 2026
https://doi.org/10.5194/acp-26-5713-2026-supplement


Atmospheric Chemistry and Physics
Open Access
EGU

*Supplement of*

# Rapid secondary organic aerosol formation at the air–water interface from methoxyphenols in wildfire emissions: UVA-driven S(IV) photooxidation to organosulfates

**Baohua Cai et al.**

*Correspondence to:* Qi Zhang (dkwzhang@ucdavis.edu) and Xin Yang (yangx@sustech.edu.cn)

**Supplementary Text**

**Preliminary experiments**

To investigate the photodegradation of guaiacol (GUA) in S(IV) solutions, a mixed aqueous solution containing 0.1 mM GUA and 2 mM $Na_2SO_3$ was irradiated under a 300 W Xe lamp with continuous stirring (Fig. S1). Preliminary experiments showed that, in the absence of air bubbling, the concentration of GUA in $Na_2SO_3$ solutions remained nearly unchanged. Air bubbling at a flow rate of 0.4 L $min^{-1}$ was introduced to maintain oxygen-saturated conditions in the reaction solution. Under dark conditions and Xe lamp irradiation with wavelengths below 400 nm filtered out, comparable GUA degradation rates were observed, which can be largely attributed to physical loss of GUA associated with continuous air bubbling at 0.4 L $min^{-1}$. In contrast, under full-spectrum Xe lamp irradiation, the degradation rate of GUA was markedly enhanced (Fig. S2), suggesting that irradiation at wavelengths below 400 nm contributes to the observed GUA degradation.

In addition, HPLC analysis revealed the formation of distinct new compounds, as evidenced by the appearance of new absorption peaks at specific retention times (Fig. S3). These results collectively indicate that UVA irradiation promotes the interaction between GUA and S(IV) in the presence of dissolved oxygen, thereby accelerating the photodegradation of GUA and leading to the formation of new reaction products.

However, the photon flux density of the Xe lamp in the UVA region is relatively low (Fig. S4A), resulting in a weak manifestation of the UVA-driven reaction process. Continued use of the Xe lamp may therefore introduce uncertainties in kinetic measurements. To obtain reliable kinetic data and enable mechanistic investigations, a high–photon-flux monochromatic UVA lamp (370 nm, Fig. S4B) was subsequently employed for detailed kinetic and mechanistic studies.

**Photon Flux Distribution in the Spherical Reactor**

The experimental irradiation setup consists of a spherical glass reactor illuminated symmetrically by two identical UVA LED lamps positioned on opposite sides. To estimate the photon flux distribution within the reactor, we consider the inverse-square law for point-like light sources:

$$I \propto \frac{1}{r^2}$$

where $I$ is the photon flux at distance $r$ from the light source.

Let $d$ denote the distance from the left lamp to the nearest point on the left side of the reactor. Consequently, the distance from the left lamp to the opposite side of the reactor (right wall) is approximately $2d$. Denoting the photon flux at the nearest point as $I$, the flux at the far side from the same lamp is:

$$I_{\text{far}} = I \times (\frac{d}{2d})^2 = \frac{1}{4}I$$

The total photon flux at the left side of the reactor is the sum of contributions from both lamps:

$$I_{\text{left}} = I_{\text{left lamp}} + I_{\text{right lamp}} = I + \frac{1}{4}I = 1.25I$$

By symmetry, the right side of the reactor experiences the same total flux:

$$I_{\text{right}} = 1.25I$$

At the center of the spherical reactor, the distance from each lamp is approximately $1.5d$. The photon flux contribution from each lamp is therefore:

$$I_{\text{center, single}} = I \times (\frac{d}{1.5d})^2 \approx 0.444I$$

The total photon flux at the center is the sum of contributions from both lamps:

$$I_{\text{center, total}} \approx 0.889I$$

**Distribution factor of GUA and aqueous phase calculation ($X_{aq}$)**

The concentrations of phenolic compounds in the gas and aqueous phases were calculated as a function of liquid water content at 5 ºC. Henry's law constant for GUA at 278 k ($K_{\text{H, 278K}}$) were calculated from the measured value at 289 K using the enthalpy of dissolution ($\Delta H_{\text{sol}}$) (Mcfall et al., 2020):

$$K_{H,278K} = K_{H,298K} \times \exp\left(\frac{\Delta H_{sol}}{R} \times \left(\frac{1}{298K} - \frac{1}{278K}\right)\right)$$

where $R$ is the ideal-gas constant (8.314 J $K^{-1}$ $mol^{-1}$). $K_{H,298K}$ is 870 M $atm^{-1}$. So that the $K_{H,278K}$ is 5326 M $atm^{-1}$.

The distribution factor ($f_{\text{phenols}}$) and the aqueous-phase fraction ($X_{aq}$) were then calculated using (John H. Seinfeld and Pandis, 2016):

$$f_{phenols} = 10^{-6} K_{H,279K} RTL$$

$$X_{aq} = \frac{f_{phenols}}{1 + f_{phenols}}$$

where $R$ = 0.08205 atm L $mol^{-1}$ $K^{-1}$; $T$ = 278 K. $L$ is the liquid water content in cloud or fog, expressed in g $m^{-3}$.

**Relative rate technique (Tran et al., 2022)**

**Experimental Methods**

All experiments were performed in a 25 mL airtight Pyrex tube with a magnetic stirrer and a bubble tube for feeding high-purity zero air or nitrogen under 370 nm light. A 20 mL reaction solution of the GUA and phenol, and $Na_2SO_3$ or $Na_2S_2O_8$. The pH of the reaction solution is regulated by $H_2SO_4$ and NaOH. The pH of solutions was measured with a pH meter REDOX potentiometer Conductivity meter (AZ-86555) that was calibrated with commercial pH standards. Aliquots of 3 mL reaction solution, to which 0.30 mL MeOH was added to stop the reaction, were sampled for chemical analysis every 15 min for 1h. Each experiment was repeated at least twice.

Model 1 experimental conditions: [guaiacol] = 0.1 mM, [phenol] = 0.1 mM, [$Na_2SO_3$] = 3.0 mM, with zero air bubbling, 370 nm light irradiation, room temperature.

Model 2 experimental conditions: [guaiacol] = 0.1 mM, [phenol] = 0.1 mM, [$Na_2S_2O_8$] = 3.0 mM, with zero air bubbling, 370 nm light irradiation, room temperature.

$$S_2O_8^{2-} + \text{UVA} \rightarrow 2SO_4^{\bullet -}$$

**The rate constant calculation**

Photodegradation correction is based on pseudo-first-order kinetics, where k is the second-order rate constant for reactions of phenol (PhOH) and guaiacol (GUA) with $SO_4^{\cdot-}$. The effective pseudo-first-order rate constants is $k' = k[SO_4^{\cdot-}]_{ss}$. and $J = 0.0016\ min^{-1}$ is the first order photolytic rate coefficient for GUA in the photodegradation control experiments (Phenol is basically non-photodegradation at 370 nm irradiation).

$$[GUA]_t = [GUA]_0 \exp\left(-(k'_{GUA} + J) \times t\right)$$
$$[PhOH]_t = [PhOH]_0 \exp\left(-k'_{phOH} \times t\right)$$

Therefore

$$\ln\frac{[GUA]_0}{[GUA]_t} = (k'_{GUA} + J) \times t$$
$$\ln\frac{[PhOH]_0}{[PhOH]_t} = k'_{phOH} \times t$$

A ratio of $k_{GUA}/k_{phOH}$ is achieved by:

$$\frac{k_{GUA}}{k_{phOH}} = \frac{k'_{GUA} + J}{k'_{phOH}} = \frac{\ln\frac{[GUA]_0}{[GUA]_t} - J \times t}{\ln\frac{[PhOH]_0}{[PhOH]_t}}$$

**Actinometry Using Potassium Ferrioxalate to Determine Photon Flux**

Experimental Procedure. 20 mL of potassium ferrioxalate solution (6 mM in 50 mM oxalic acid) was irradiated for 10 s. Immediately after irradiation, 1 mL of the reaction solution was mixed with 1 mL of pH 3 buffer (prepared from acetic acid/sodium acetate) and 1 mL of o-phenanthroline·HCl solution (0.1% w/v) to allow color development (total volume 3 mL). Then, 1 mL of the colored solution was diluted with 9 mL of water, and the absorbance at 510 nm was measured in a 1 cm pathlength cuvette. All experiments were conducted at room temperature, and the colorimetric reaction was performed immediately to prevent oxidation of $Fe^{2+}$.

Photon Flux Calculation. The measured absorbance of the diluted solution (A = 0.403) was used to calculate the $Fe^{2+}$ concentration using the molar absorptivity $\varepsilon = 1.11 \times 10^4\ L\ mol^{-1}\ cm^{-1}$. Considering the dilution factors and the 20 mL reaction volume, the total moles of $Fe^{2+}$ formed during irradiation were determined. Using the quantum yield for potassium ferrioxalate at 365 nm ($\Phi = 1.11$), the total number of absorbed photons was calculated by $N\_photons = n(Fe^{2+})/\Phi$. The photon flux was then obtained by dividing by the irradiation time (t = 10 s), total photon flux (photons/s) is $1.17 \times 10^{18}$ photons $s^{-1}$.

**Estimation of Apparent Photon Efficiency (APE) for S(IV) oxidation**

The apparent photon efficiency (APE) of S(IV) oxidation was estimated based on the experimentally measured pseudo-first-order rate constant under controlled irradiation conditions. Here, APE is defined as the number of S(IV) molecules oxidized per incident photon, and thus represents a condition-dependent, process-level measure of photochemical reactivity under the specific experimental configuration, rather than an intrinsic photochemical quantum yield. This definition is intended to avoid overinterpretation and to distinguish APE from standardized quantum efficiency metrics. The calculation was performed as follows:

$$APE = \frac{S(IV)\ reaction\ rate\ (molecules/s)}{total\ photon\ flux\ (photons/s)}$$

Experimental conditions: The experiments were conducted in a circular glass vessel with a diameter of 4 cm and a reaction volume of 20 mL. The initial concentration of S(IV) was 0.5 mM. The solution was irradiated with a single-wavelength UVA light source (maximum intensity at 370 nm) providing a photon flux of $1.59\times10^{17}$ photons $cm^{-2}$ $s^{-1}$, while continuously stirred to maintain homogeneous reaction conditions. The apparent degradation rate of S(IV) under these conditions was determined from the observed concentration changes over time.

$$S(IV)\ reaction\ rate\ (molecules/s)\ = k_{obs} \times C_0 \times V \times N_A$$
$$total\ photon\ flux\ (photons/s))\ = I \times A$$
$$APE = \frac{k_{obs} \times C_0 \times V \times N_A}{I \times A} = \frac{0.5\ \times 10^{-3} M \times 20 \times 10^{-3}\ L\ \times 6.022 \times 10^{23}}{1.59 \times 10^{17} \text{photons}\ cm^{-2}s^{-1} \times 3.14 \times (2\ cm)^2} \times k_{obs}$$
$$APE = 3.02 \times k_{obs}$$

Assuming that the apparent photon efficiency (APE) of S(IV) photooxidation under UVA irradiation remains constant, a cloud-droplet-representative liquid water content was adopted to provide an upper-limit estimate. The UVA photon flux (300nm-400nm) was taken from the AM0 standard solar spectrum ($1.67 \times 10^{16}$ photons $cm^{-2}$ $s^{-1}$) to assess the sensitivity of S(IV) photooxidation under strong solar irradiation conditions (Fig. S4). For an assumed liquid water content (LWC) of 0.1 g $m^{-3}$, the total liquid water volume in 1 $m^3$ of air is $1.0 \times 10^{-7}$ $m^3$. If this volume is idealized as a single spherical droplet, the equivalent droplet diameter is approximately 5.8 mm, corresponding to an illuminated cross-sectional area of $2.6 \times 10^{-5}$ $m^2$ (0.26 $cm^2$). Using the empirically fitted pH-dependent S(IV) photooxidation rate under UVA irradiation (Fig. S10), the resulting relationship between the apparent rate constant ($k_{obs}$), pH, and the S(IV) concentration ([S(IV)]) was finally obtained.

$$k_{obs} = \frac{APE \times I \times A}{C_0 \times V \times N_A}$$
$$= \frac{3.02\ \times 1.75 \times 10^{-8} \times pH^{6.23} \times 1.67 \times 10^{16} \text{photons}\ cm^{-2}s^{-1} \times 0.26\ cm^2}{S(IV)(M) \times 1.0 \times 10^{-4} L \times 6.022 \times 10^{23}}$$
$$k_{obs} = \frac{3.8 \times 10^{-12} \times pH^{6.23}}{S(IV)\ (M)} s^{-1}$$

The photolysis of $NO_2$ is primarily driven by radiation in the UVA spectral region. Previous studies have shown that under haze conditions, the photolysis efficiency of $NO_2$ can be reduced by up to 66% (Hollaway et al., 2019). Therefore, the actinic photon flux under haze conditions was estimated by applying a 66% reduction, resulting in a value of $5.68 \times 10^{15}$ photons $cm^{-2}$ $s^{-1}$. For an assumed liquid water content (LWC) of 300 μg $m^{-3}$, the total liquid water volume in 1 $m^3$ of air is $3.0 \times 10^{-10}$ $m^3$. If this volume is idealized as a single spherical droplet, the equivalent droplet diameter is approximately 0.82 mm, corresponding to an illuminated cross-sectional area of $5.3 \times 10^{-7}$ $m^2$ ($5.3 \times 10^{-3}$ $cm^2$). The APE under these conditions was then calculated as follows:

$$k_{obs} = \frac{APE \times I \times A}{C_0 \times V \times N_A}$$

$$= \frac{3.02 \times 1.75 \times 10^{-8} \times pH^{6.23} \times 5.68 \times 10^{15} \text{photons}\, cm^{-2} s^{-1} \times 5.3 \times 10^{-3}\, cm^2}{S(IV)(M) \times 3.0 \times 10^{-7}\, L \times 6.022 \times 10^{23}}$$

$$k_{obs} = \frac{8.8 \times 10^{-12} \times pH^{6.23}}{S(IV)\,(M)} s^{-1}$$

**Coordinates of the structure**

$SO_3^{2-}$:

S 0.00015600 0.00018800 0.36151200
O 1.38572000 -0.24335000 -0.24107700
O -0.48223400 1.32083300 -0.24107800
O -0.90379800 -1.07785700 -0.24086900

Sum of electronic energy and thermal correction to G: -623.4450423 a.u.

$O_2$:

O 0.00000000 0.00000000 0.59360300
O 0.00000000 0.00000000 -0.59360300

Sum of electronic energy and thermal correction to G: -150.1566305 a.u.

[$SO_3^{2-}$ + $O_2$]:

S 0.96864400 -0.04418400 -0.20653100
O 2.38919700 -0.44069500 -0.61297600
O 1.06524600 1.41394400 0.24872600
O 0.66735600 -0.84784400 1.05959300
O -2.94989700 0.52084100 0.09346400
O -3.10919000 -0.55787800 -0.37574400

Sum of electronic energy and thermal correction to G: -773.5908018 a.u.

$SO_3^{\cdot-}$:

S 0.00001100 -0.00005500 0.23076000
O 1.26234500 -0.64995800 -0.15385200
O -0.06818600 1.41809700 -0.15382000
O -1.19418100 -0.76802900 -0.15384700

Sum of electronic energy and thermal correction to G: -623.2845358 a.u.

$O_2^{\cdot-}$:

O 0.00000000 0.00000000 0.65791100
O 0.00000000 0.00000000 -0.65791100

Sum of electronic energy and thermal correction to G: -150.2964283 a.u.

$SO_5^{\cdot-}$:

S 0.45122400 0.14219000 0.00000000
O 0.73865300 1.54990000 0.00000000
O 0.73865300 -0.56776700 1.21625700
O 0.73865300 -0.56776700 -1.21625700
O -1.28477600 0.23510800 0.00000000
O -1.83363100 -0.93385400 0.00000000

Sum of electronic energy and thermal correction to G: -773.4558495 a.u.

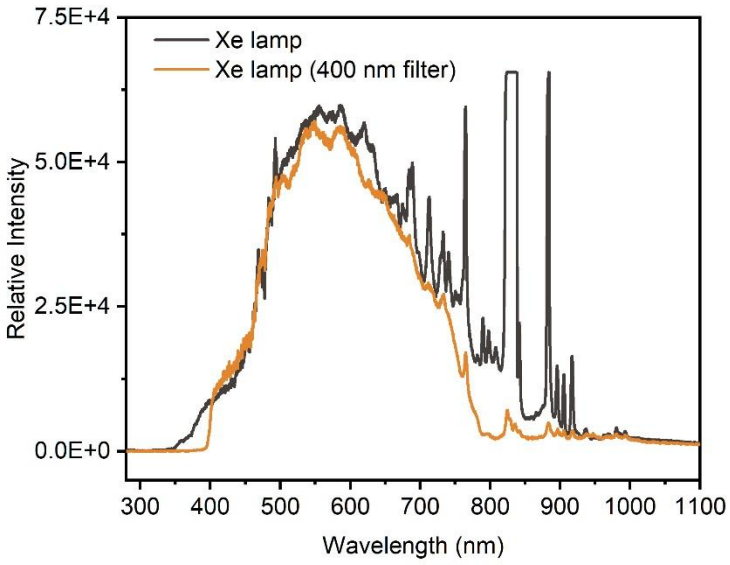


**Fig. S1.** Emission spectra of the Xe lamp and the Xe lamp equipped with a 400 nm cutoff filter.

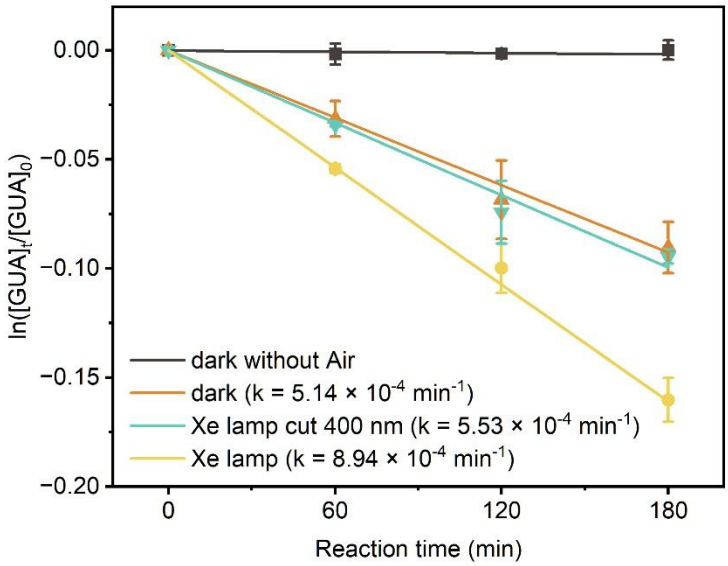


**Fig. S2.** The pseudo-first-order rate constant for the photodegradation of GUA in $Na_2SO_3$ solutions under different irradiation conditions. Error bars represent the standard deviation from at least two independent experiments. Experimental conditions: [guaiacol] = 0.1 mM, [$Na_2SO_3$] = 2.0 mM, pH = 4.0 ± 0.1, zero-air bubbling, Xe lamp irradiation, room temperature.

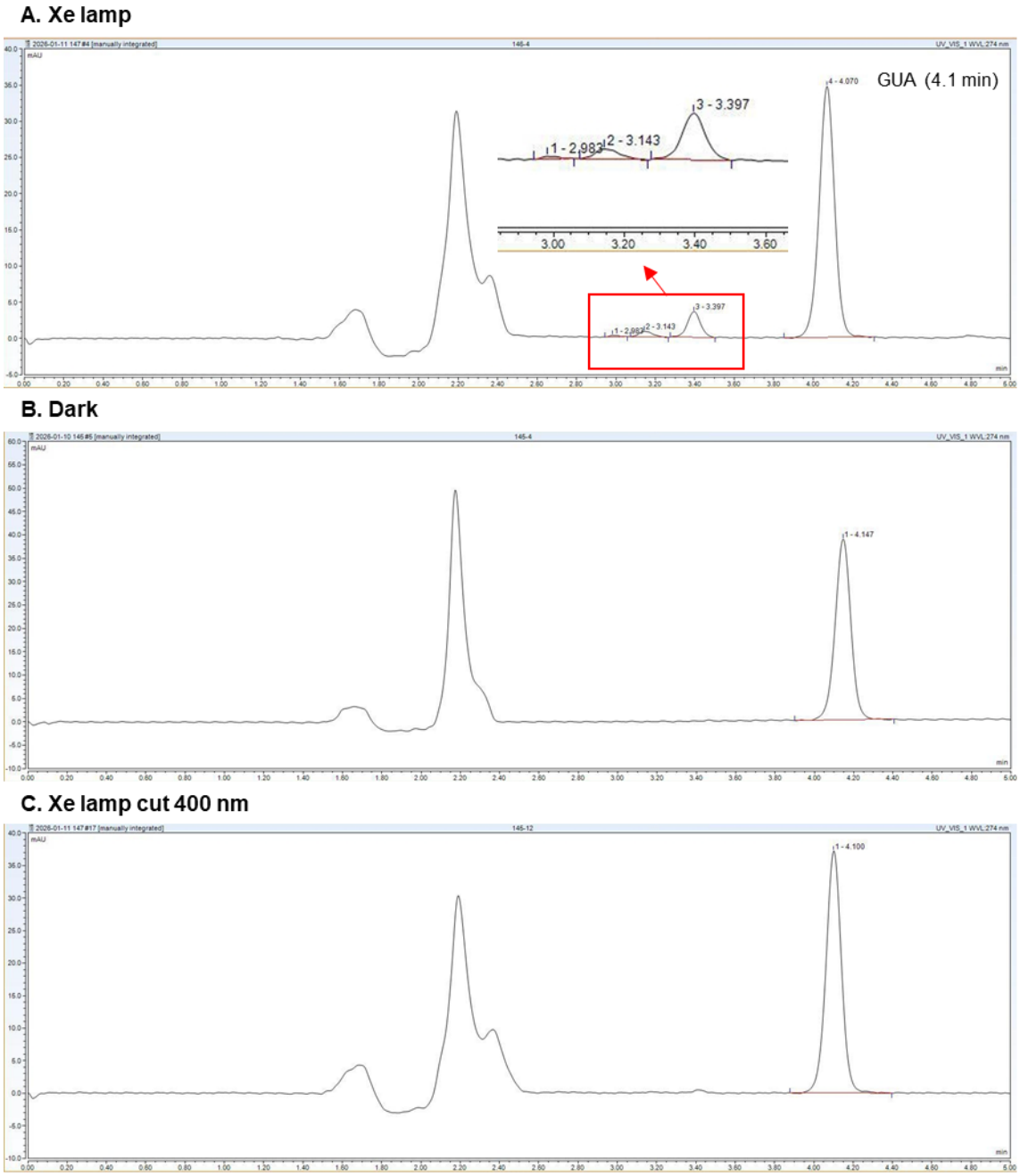


**Fig. S3.** HPLC chromatograms of the reaction mixture after 180 min of reaction under different irradiation conditions: (A) Xe lamp irradiation; (B) dark condition; (C) Xe lamp irradiation with a 400 nm cutoff filter.

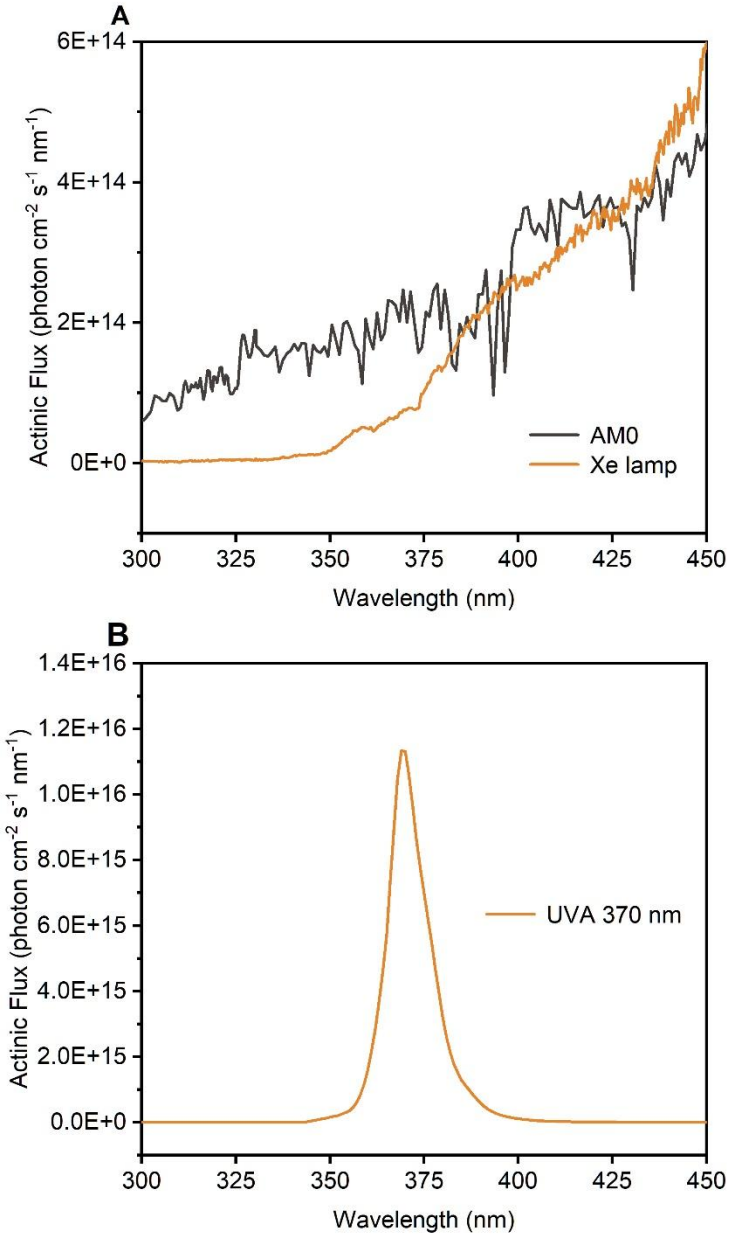


**Fig. S4.** (A) Actinic flux of the AM0 standard solar spectrum and the xenon lamp (Beijing Perfectlight Technology Co., Ltd.). (B) Actinic flux of the Kessil PR160L-370 nm lamp


**Fig. S5.** The glass instrument was used in the experiment.

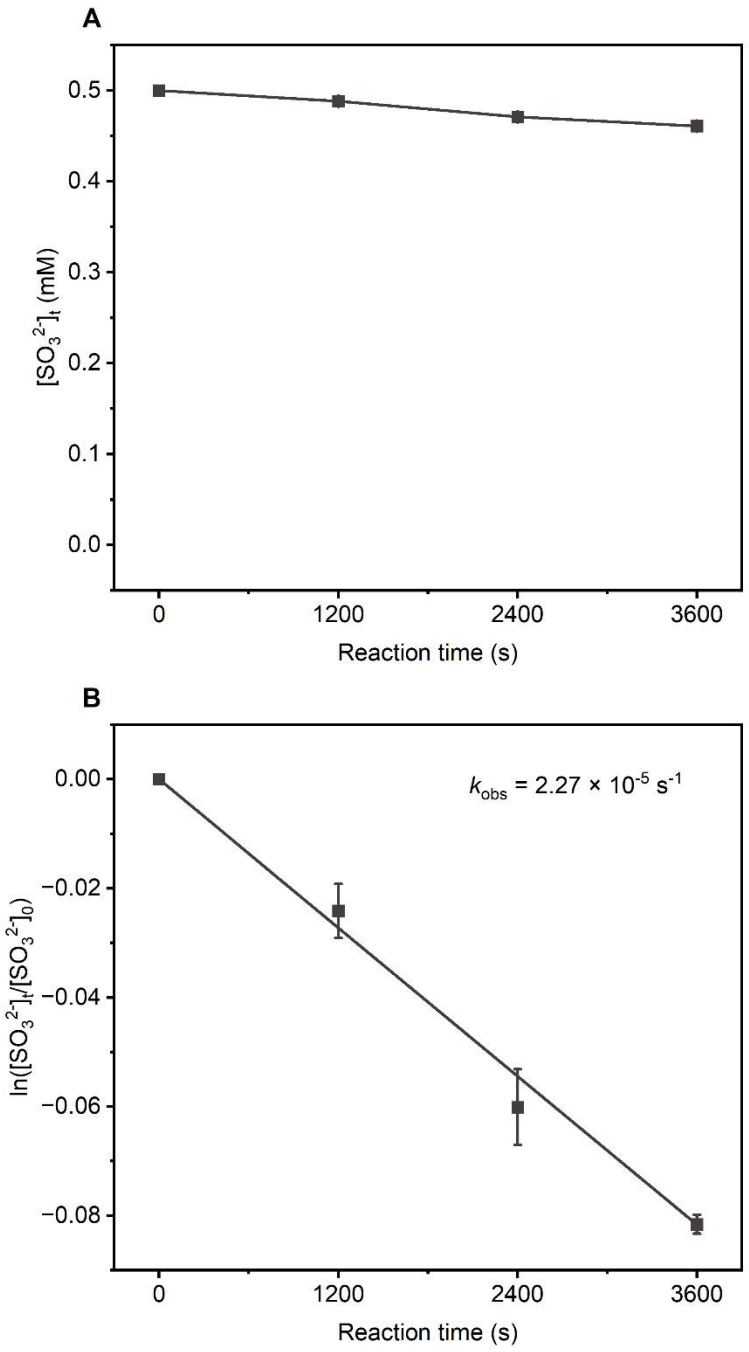


**Fig. S6.** (A) Kinetics of the aqueous-phase oxidation of $SO_3^{2-}$ under dark conditions. (B) The pseudo-first-order rate constant for the oxidation of $Na_2SO_3$. Error bars represent the standard deviation from at least two independent experiments. Experimental conditions: [$Na_2SO_3$] = 0.5 mM, pH = 4.0 ± 0.1, zero-air bubbling, room temperature, Solution acidity was controlled using a phosphoric acid / phosphate buffer system.

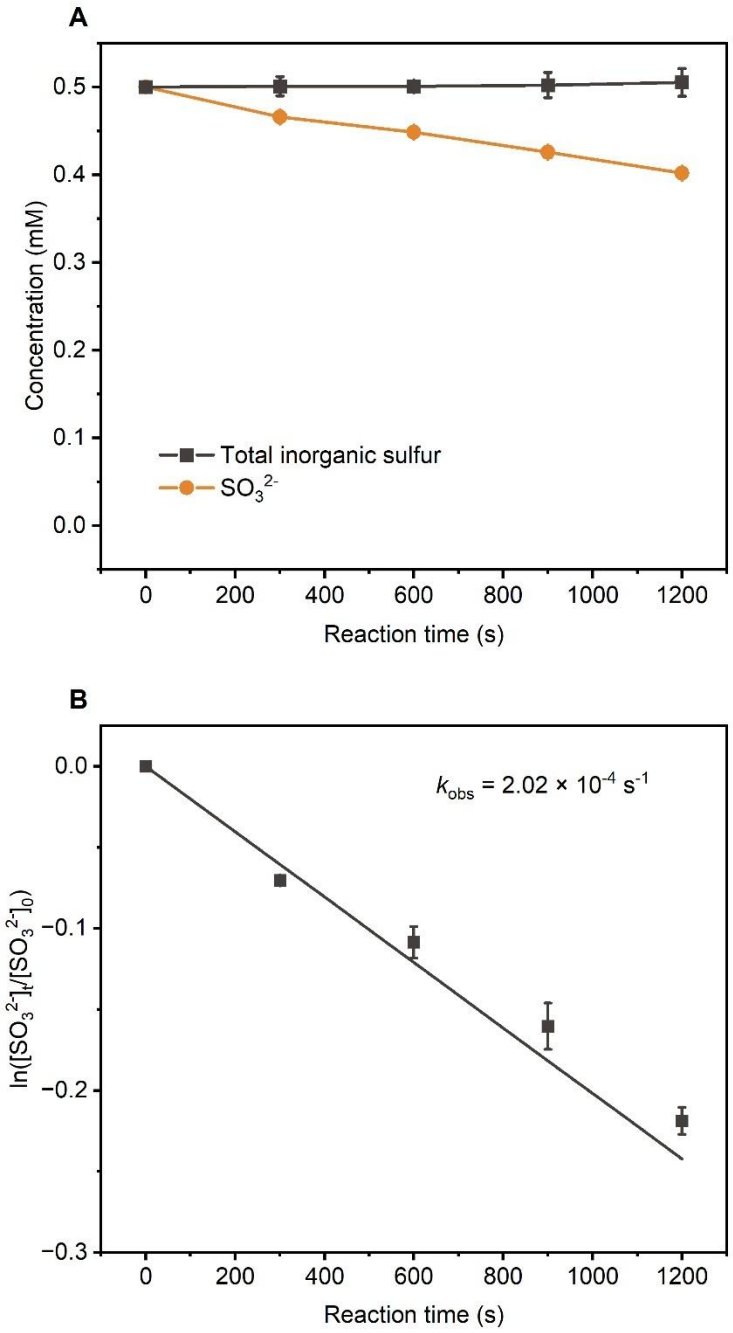


**Fig. S7.** (A) Kinetics of the aqueous-phase oxidation of $SO_3^{2-}$ under 370 nm irradiation. (B) The pseudo-first-order rate constant for the photooxidation of $Na_2SO_3$. Error bars represent the standard deviation from at least two independent experiments. Experimental conditions: [$Na_2SO_3$] = 0.5 mM, pH = 4.0 ± 0.1, zero-air bubbling, 370 nm light irradiation, room temperature. Solution acidity was controlled using a phosphoric acid / phosphate buffer system.

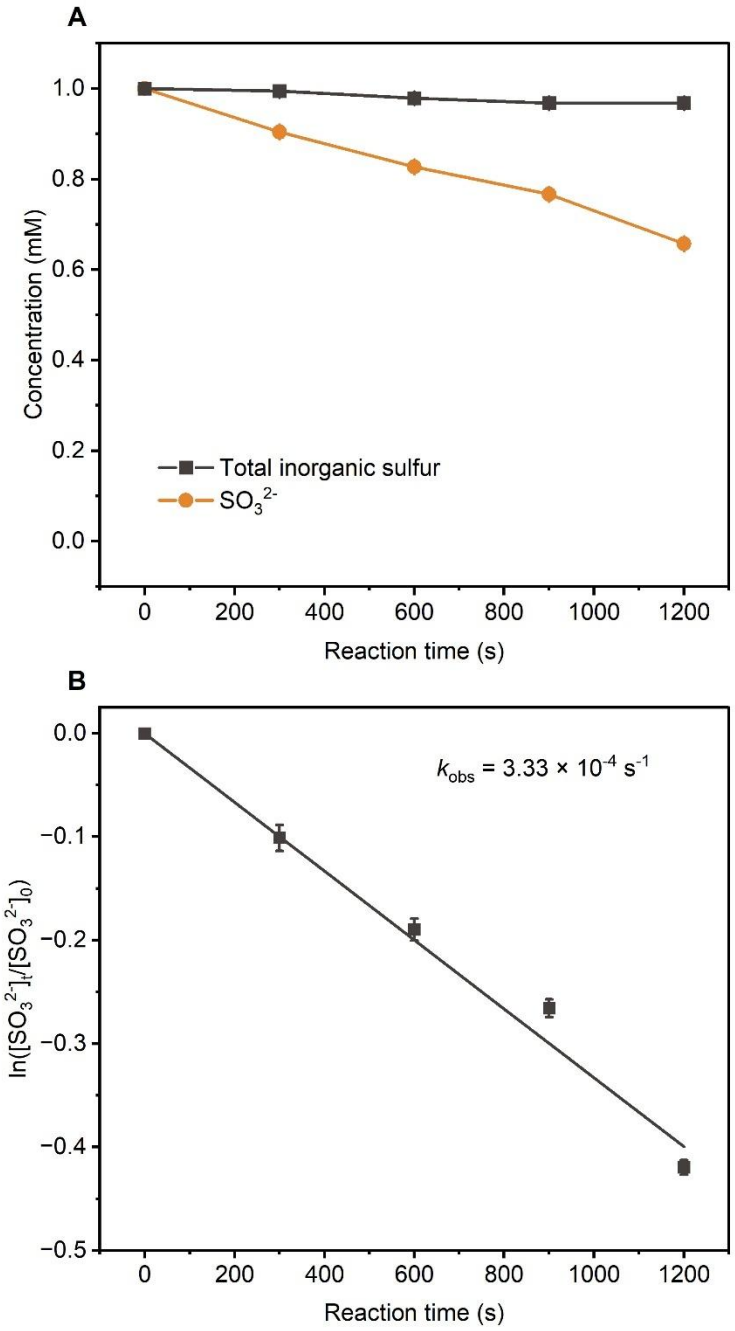


**Fig. S8.** (A) Kinetics of the aqueous-phase oxidation of $SO_3^{2-}$ under 370 nm irradiation. (B) The pseudo-first-order rate constant for the photooxidation of $Na_2SO_3$. Error bars represent the standard deviation from at least two independent experiments. Experimental conditions: [$Na_2SO_3$] = 1.0 mM, pH = 4.0 ± 0.1, zero-air bubbling, 370 nm light irradiation, room temperature. Solution acidity was controlled using a phosphoric acid / phosphate buffer system.

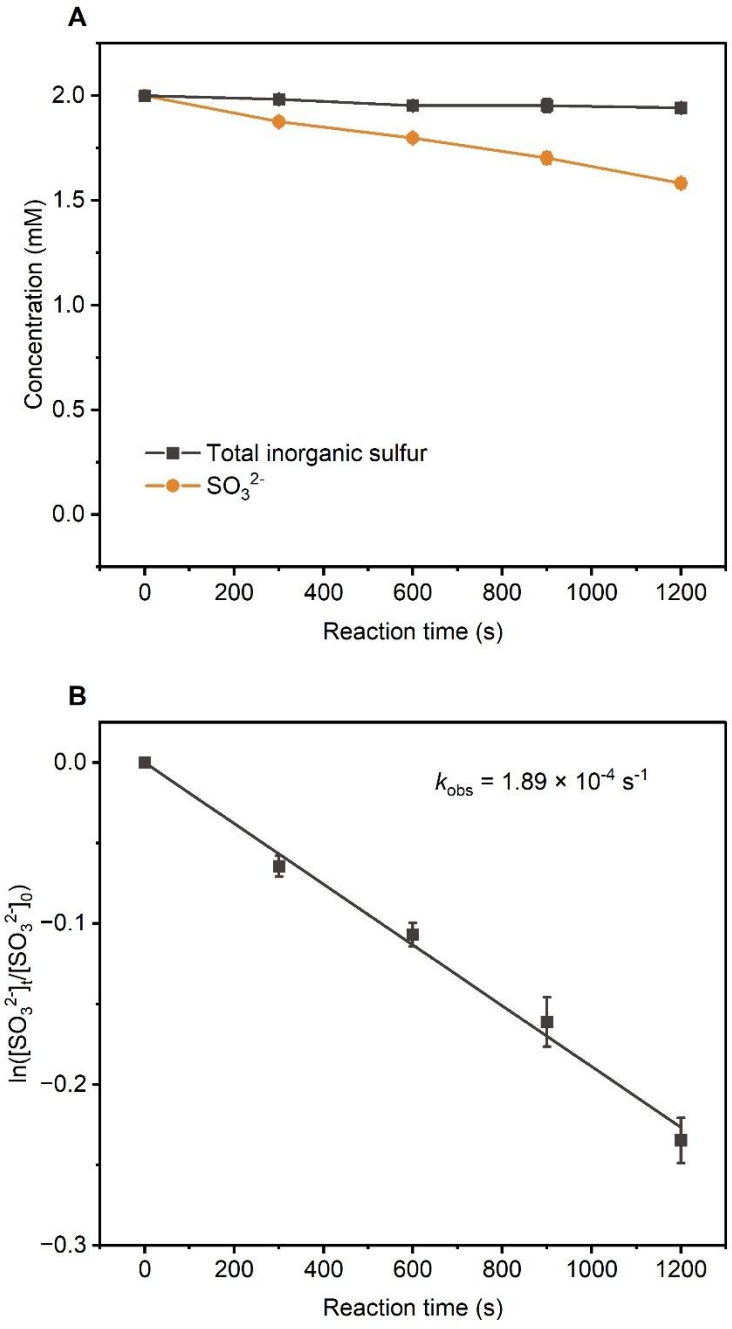


**Fig. S9.** (A) Kinetics of the aqueous-phase oxidation of $SO_3^{2-}$ under 370 nm irradiation. (B) The pseudo-first-order rate constant for the photooxidation of $Na_2SO_3$. Error bars represent the standard deviation from at least two independent experiments. Experimental conditions: [$Na_2SO_3$] = 2.0 mM, pH = 4.0 ± 0.1, zero-air bubbling, 370 nm light irradiation, room temperature. Solution acidity was controlled using a phosphoric acid / phosphate buffer system.

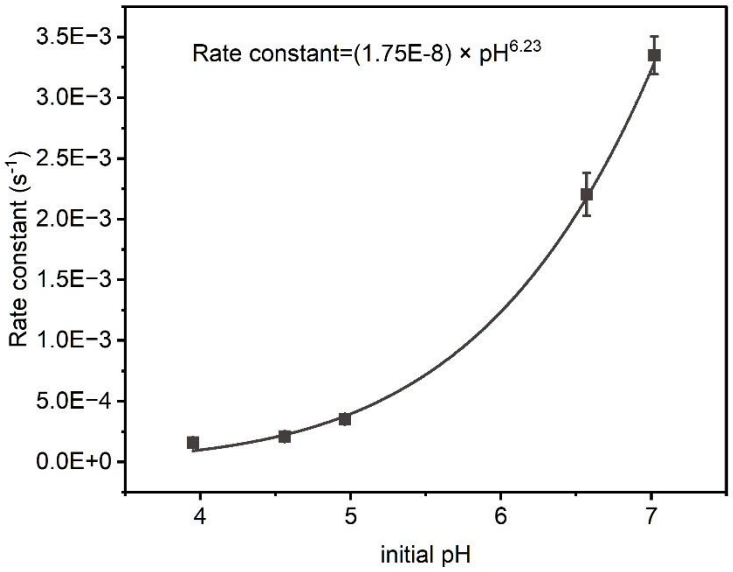


**Fig. S10.** Variation in the oxidation rate constants for $SO_3^{2-}$ under 370 nm light as a function of initial pH. Error bars represent the standard deviation from at least two independent experiments. Experimental conditions: [$Na_2SO_3$] = 0.5 mM, zero-air bubbling, 370 nm light, room temperature. Solution acidity was controlled using a phosphoric acid / phosphate buffer system.

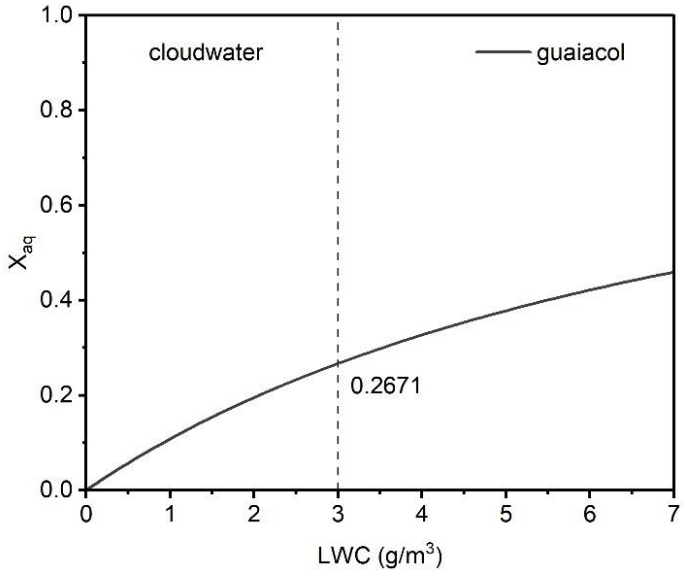


**Fig. S11.** The gas-water distribution of GUA under an air temperature of 5 ºC and varying liquid water content.

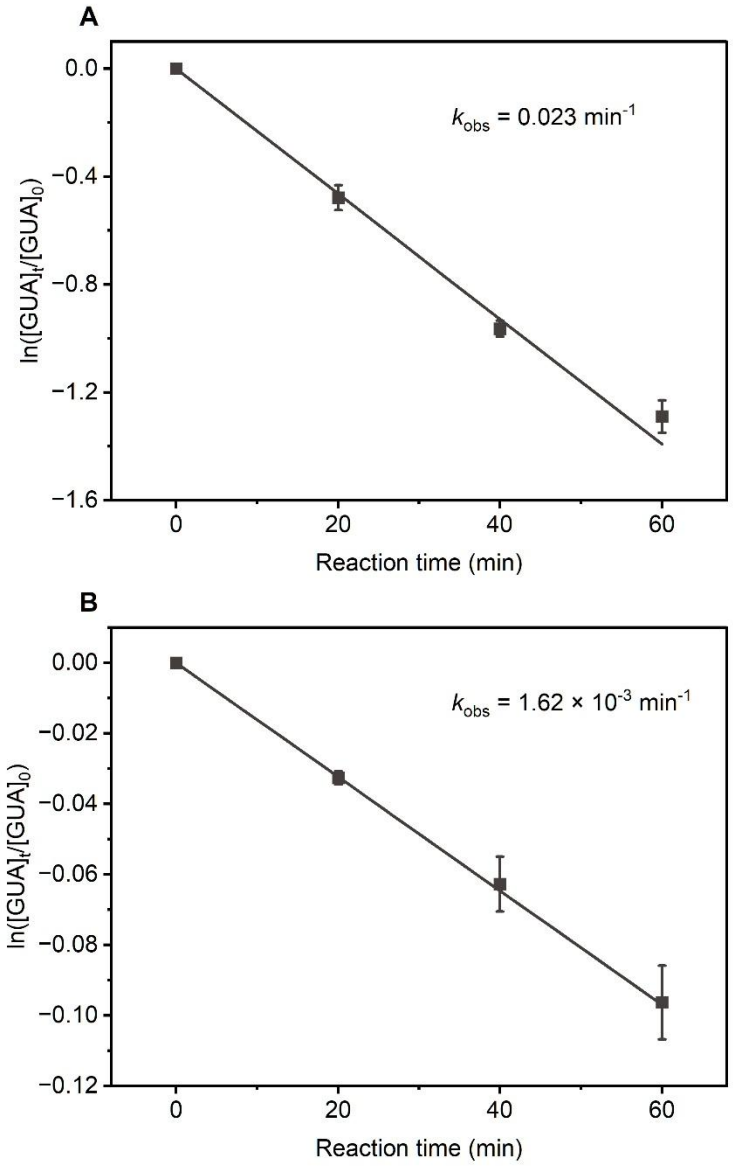


**Fig. S12.** (A) The pseudo-first-order rate constant for the reaction between GUA and $Na_2SO_3$ under 370 nm irradiation. (B) The pseudo-first-order rate constant for the photooxidation of GUA under 370 nm irradiation. Error bars represent the standard deviation from at least two independent experiments. Experimental conditions: [guaiacol] = 0.1 mM, [$Na_2SO_3$] = 2.0 mM, pH = 4.0 ± 0.1, with zero-air bubbling, 370 nm light irradiation, room temperature.

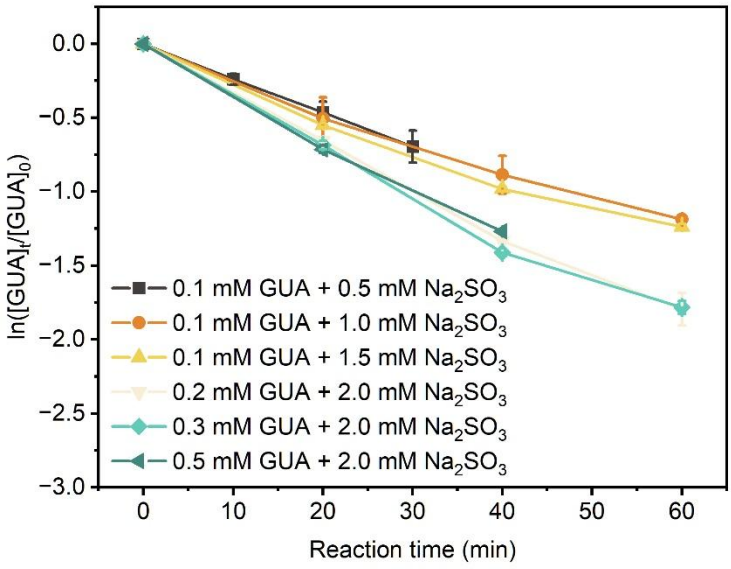


**Fig. S13.** Reaction kinetics of guaiacol degradation in aqueous solution as a function of $Na_2SO_3$ concentration. Error bars represent the standard deviation from at least two independent experiments. Experimental conditions: [guaiacol] = 0.1 mM, pH = 4.0 ± 0.1, zero-air bubbling, 370 nm irradiation, room temperature.

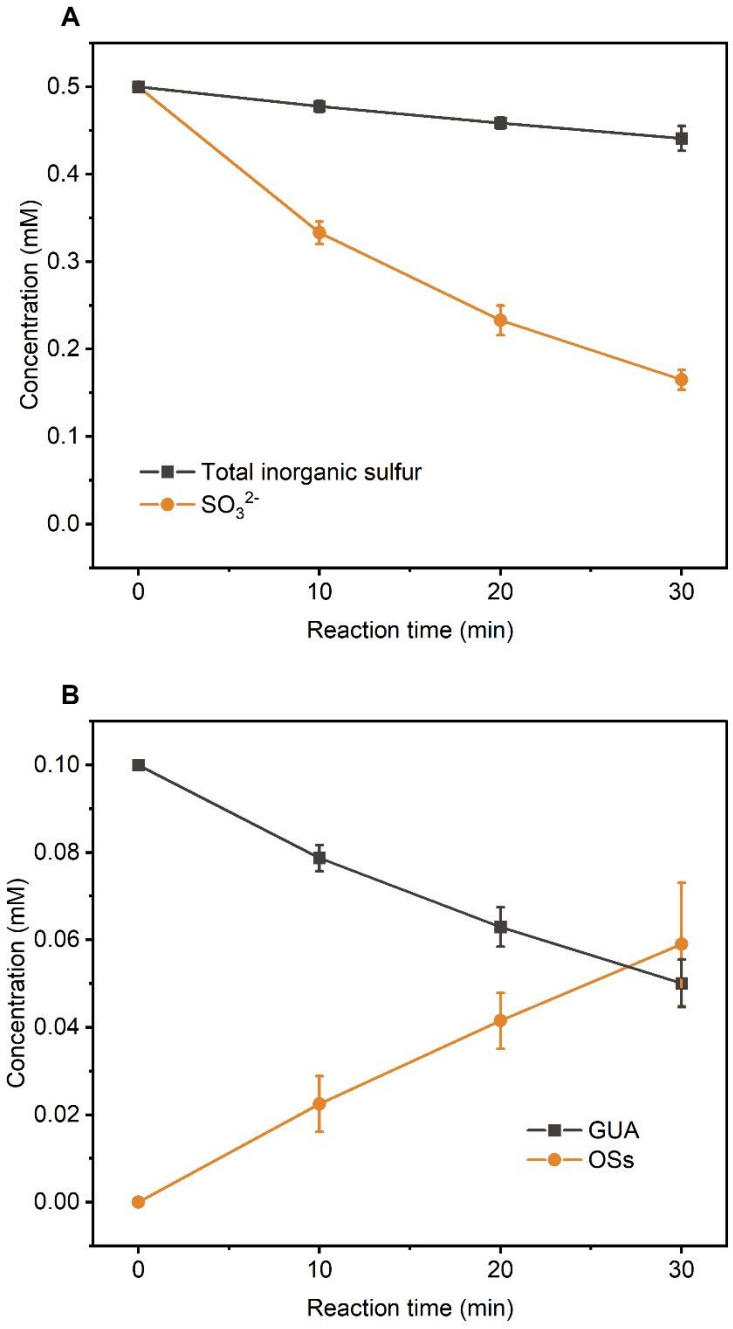


**Fig. S14.** Kinetics of the aqueous-phase reaction between guaiacol and $Na_2SO_3$ under 370 nm irradiation. (A) Time evolution of $SO_3^{2-}$ and total inorganic sulfur. (B) Concentrations of guaiacol and estimated organosulfates (OSs) over time. [OSs] = 0.5 mM – [total inorganic sulfur], where 0.5 mM is the initial concentration of $SO_3^{2-}$. Error bars represent the standard deviation from at least two independent experiments. Experimental conditions: [guaiacol] = 0.1 mM, $[Na_2SO_3]_0$ = 0.5 mM, pH = 4.0 ± 0.1, zero-air bubbling, 370 nm light irradiation, room temperature. Solution acidity was controlled using a phosphoric acid / phosphate buffer system.

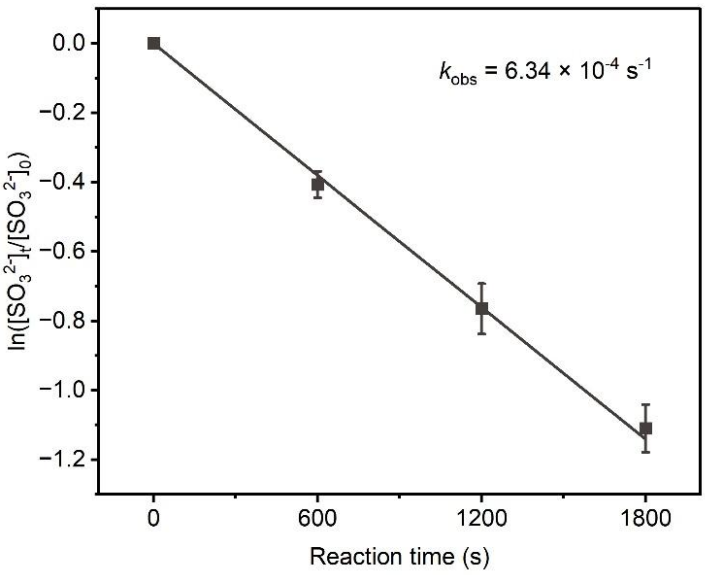


**Fig. S15.** Pseudo-first-order rate constant for the photooxidation of $Na_2SO_3$ in the presence of GUA. Error bars represent the standard deviation from at least two independent experiments. Experimental conditions: [GUA] = 0.1 mM, [$Na_2SO_3$] = 0.5 mM, pH = 4.0 ± 0.1, zero-air bubbling, 370 nm irradiation, room temperature. Solution acidity was controlled using a phosphoric acid / phosphate buffer system.

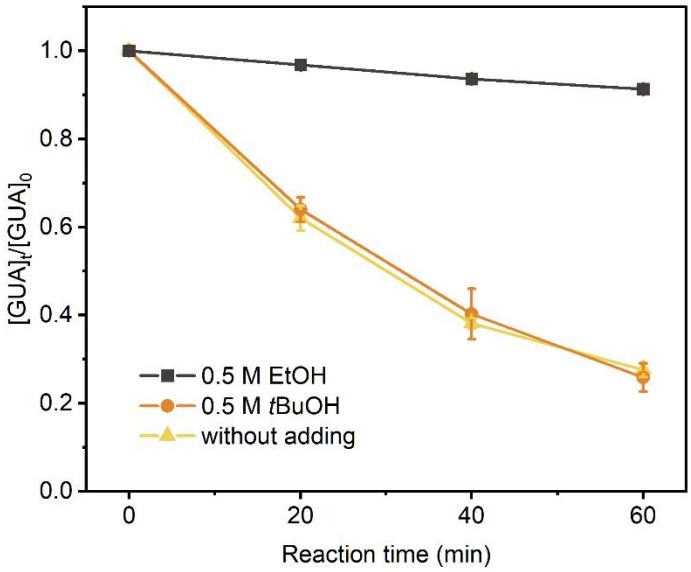


**Fig. S16.** Kinetics of the aqueous-phase reaction between guaiacol and $Na_2SO_3$ under 370 nm irradiation in the presence of different radical quenchers. Error bars represent the standard deviation from at least two independent experiments. Experimental conditions: [guaiacol] = 0.1 mM, [$Na_2SO_3$] = 2.0 mM, [EtOH] = 0.5 M, [*t*BuOH] = 0.5 M, pH = 4.0 ± 0.1, zero-air bubbling, 370 nm irradiation, room temperature.

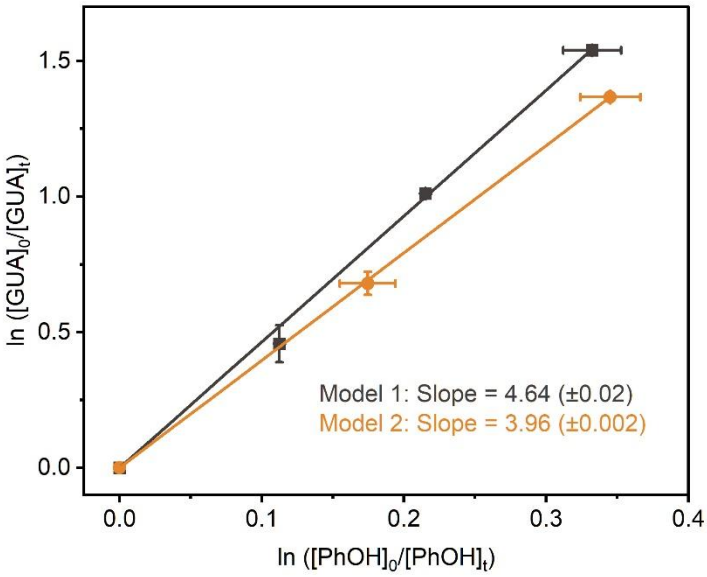


**Fig. S17.** Relative rate determination of GUA vs. phenol (PhOH) under two conditions: Model 1 – 0.1 mM GUA, 0.1 mM PhOH, and 3.0 mM $Na_2SO_3$; Model 2 – 0.1 mM GUA, 0.1 mM PhOH, and 3.0 mM $Na_2S_2O_8$. Error bars represent the standard deviation from at least two independent experiments. Experimental conditions: zero-air bubbling, 370 nm irradiation, room temperature.

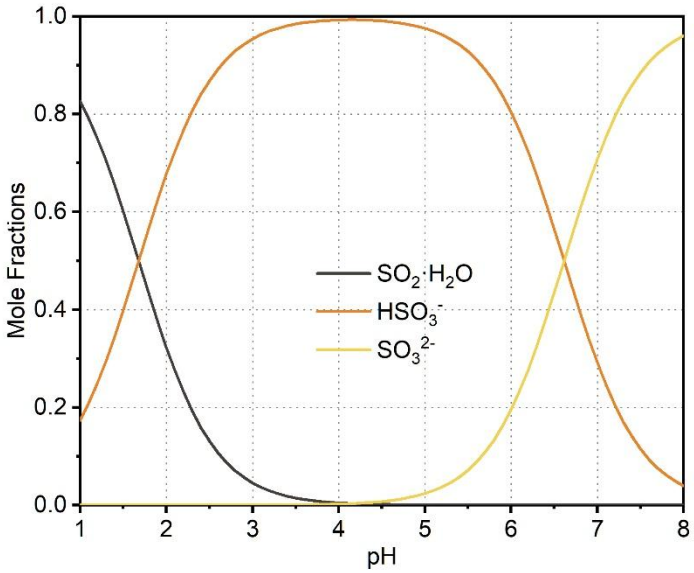


**Fig. S18.** Speciation of S(IV) inorganic compounds based on their pKa values.

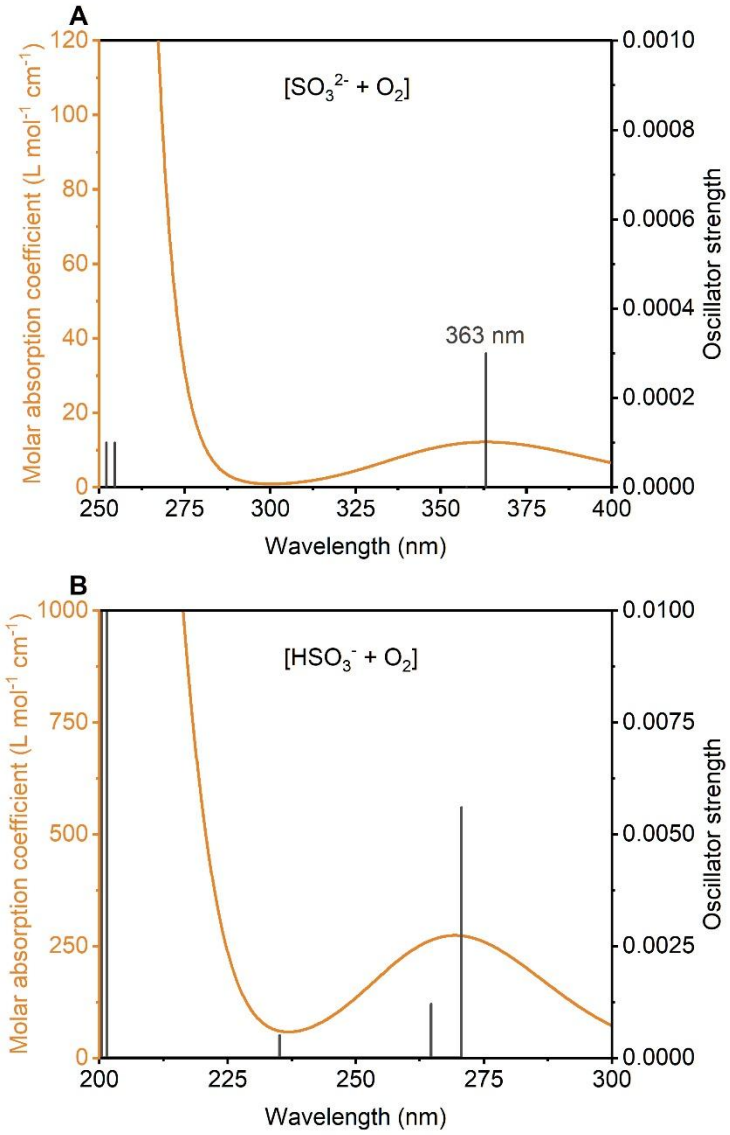


**Fig. S19.** Vertical excitation spectra. A [$SO_3^{2-}$ + $O_2$] complex and B [$HSO_3^-$ + $O_2$] complex, calculated using TDDFT at the M06-2X/ma-TZVP/SMD(water) level.

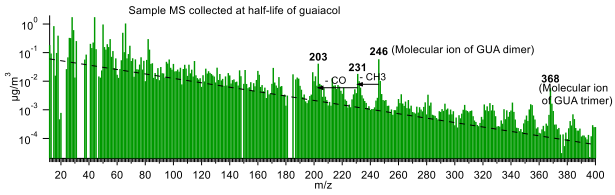


**Fig. S20.** High-resolution aerosol mass spectrum (HR-ToF-AMS) of low-volatility organics in the sample solution following 50% guaiacol depletion, obtained from the experiment with 0.5 mM guaiacol, 0.5 mM $Na_2SO_3$, 0.48 mM $H_2SO_4$. Peaks corresponding to the GUA dimer, its fragment ions, and trimer ions are indicated. The broken line is added to guide the eye

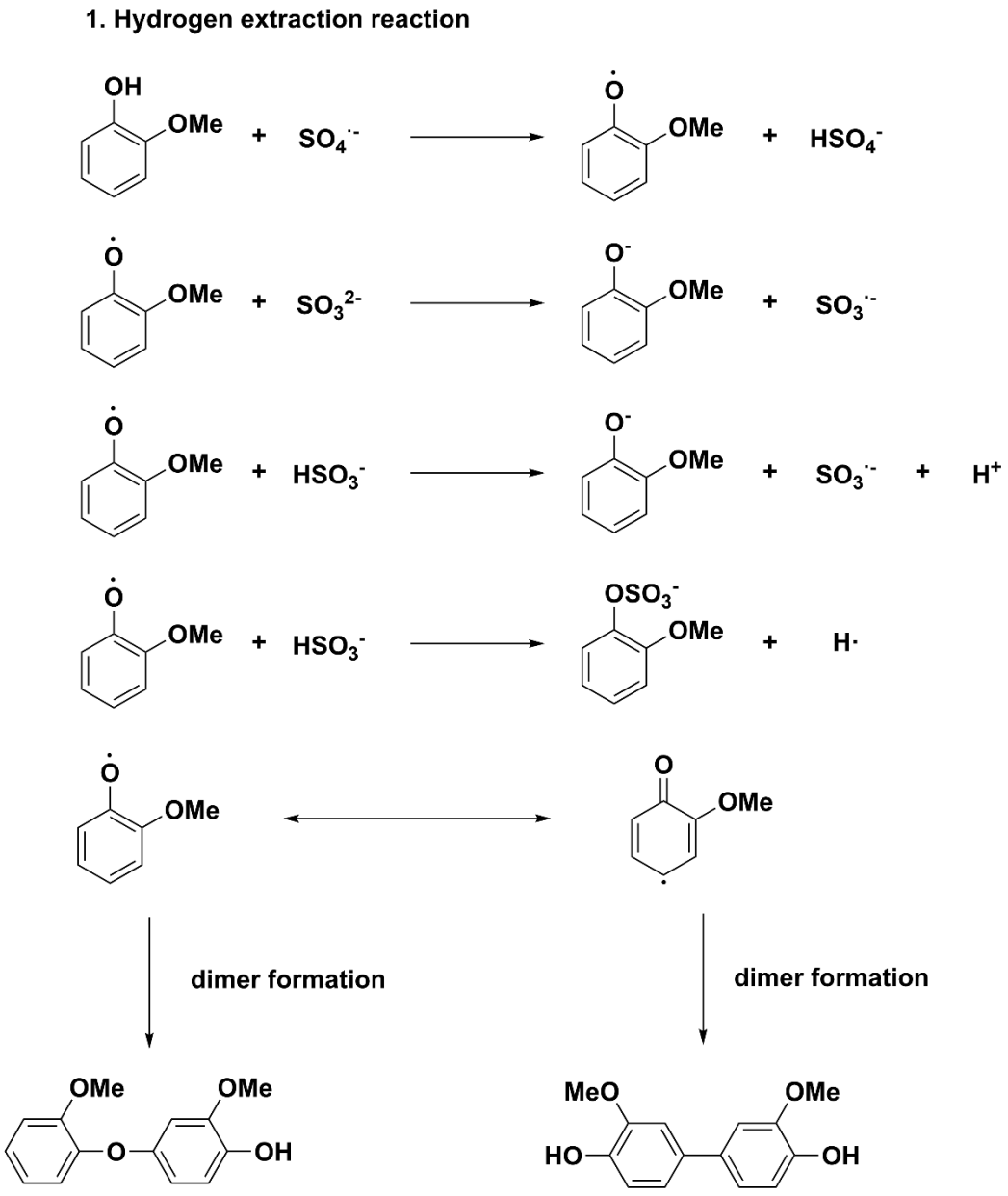


**Fig. S21.** The possible reaction mechanism between GUA and $SO_4^{\bullet-}$.

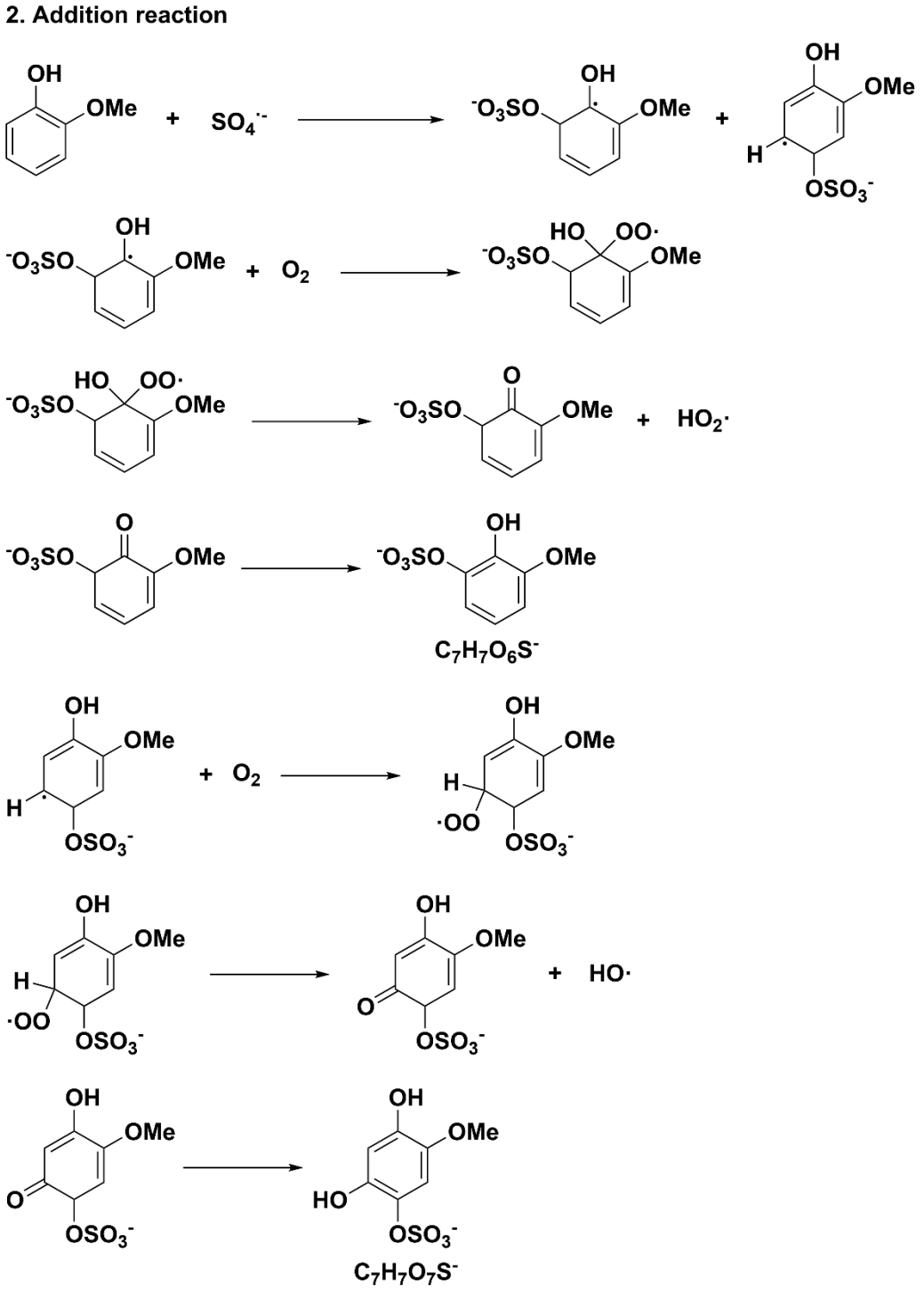


**Fig. S22.** The possible reaction mechanism between GUA and $SO_4^{\bullet-}$.

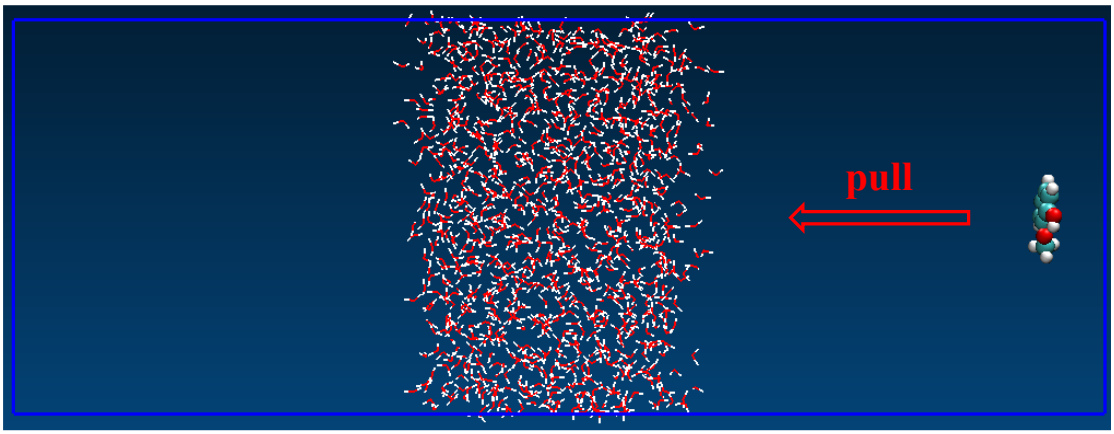


**Fig. S23.** Classical molecular dynamics simulation uses the Weighted Histogram Analysis Method (WHAM) to calculate the potential of mean force (PMF). GUA was positioned at coordinates (1.8, 1.8, 9.5 nm), while water clusters were centered in the simulation box at (3.6, 3.6, 10 nm) with a thickness of 2.35 nm. The white, red and dark cyan balls symbolize H, O, and C atoms, respectively.

**A**

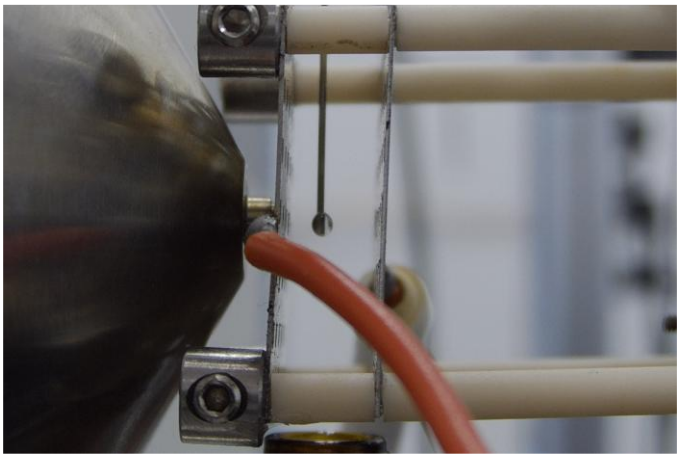

**B**

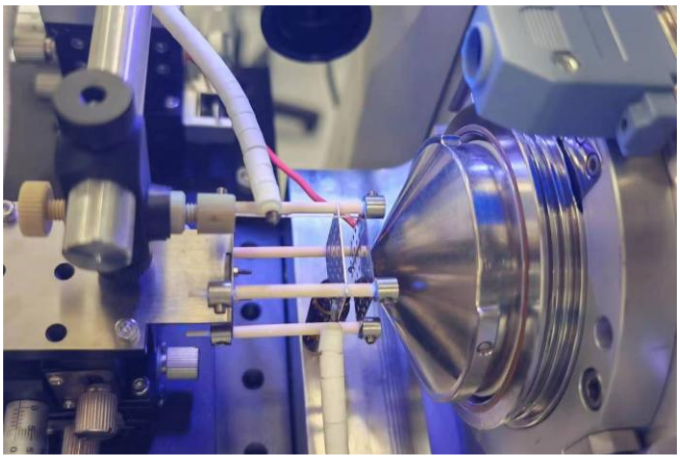

**Fig. S24.** FIDI-MS setup used to investigate the photodegradation of GUA and $Na_2SO_3$ under 370 nm irradiation.

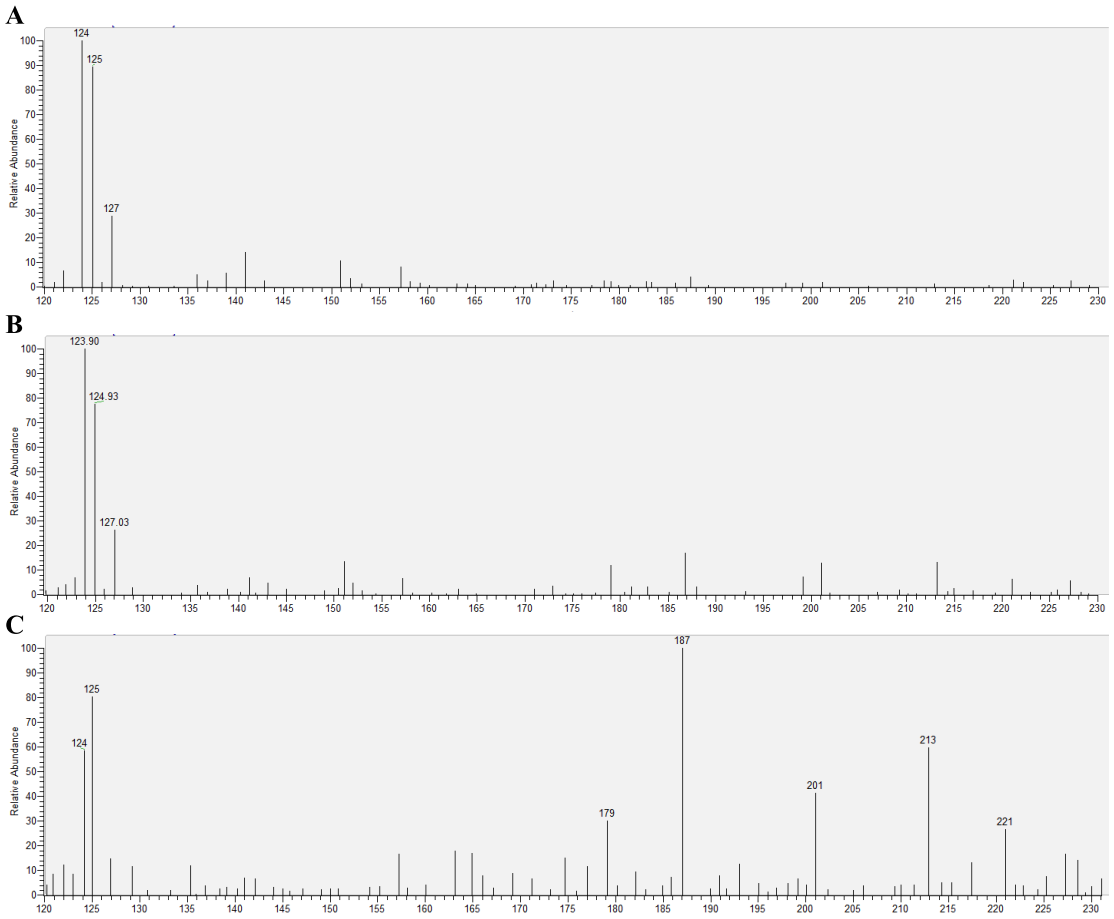


**Fig. S25.** FIDI-MS analysis of the photodegradation of GUA and $Na_2SO_3$ under 370 nm irradiation. (A) Mass spectrum of 0.1 mM GUA solution droplets after exposure to air for 2 minutes without irradiation. (B) Mass spectrum of 0.1 mM GUA solution droplets exposed to air for 1 minute followed by 1 minute for 370 nm irradiation. (C) Mass spectrum of 0.1 mM GUA and 3.0 mM $Na_2SO_3$ solution droplets exposed to air for 1 minute and then irradiated at 370 nm for 1 minute.

**Table S1.** The S(IV) oxidation reaction with $H_2O_2$ and its rate constant (John H. Seinfeld and Pandis, 2016).

| **Reaction** | ***k*** ($M^{-1}$ $s^{-1)}$ |
|---|---|
| $O_2^{\bullet-} + H^+ \rightarrow HO_2\bullet$ | $3.56 \times 10^{10}$ |
| $HO_2\bullet + HO_2\bullet \rightarrow H_2O_2 + O_2$ | $8.6 \times 10^5$ |
| $S(IV) + O_2^{\bullet-} + H2O \rightarrow S(VI) + OH\bullet + OH^-$ | $1.0 \times 10^5$ |
| $S(IV) + HO_2\bullet \rightarrow S(VI) + OH\bullet$ | $1.0 \times 10^6$ |
| $S(IV) + OH\bullet \rightarrow S(VI) + OH\bullet$ | $4.5 \times 10^9$ |
| $S(IV) + H_2O_2 \rightarrow S(VI) + H_2O$ | $7.5 \times 10^7$ |

**References**

Hollaway, M., Wild, O., Yang, T., Sun, Y., Xu, W., Xie, C., Whalley, L., Slater, E., Heard, D., and Liu, D.: Photochemical impacts of haze pollution in an urban environment, Atmos. Chem. Phys., 19, 9699–9714, 10.5194/acp-19-9699-2019, 2019.

John H. Seinfeld and Pandis, S. N.: ATMOSPHERIC CHEMISTRY AND PHYSICS From Air Pollution to Climate Change Third Edition, Wiley2016.

McFall, A. S., Johnson, A. W., and Anastasio, C.: Air–Water Partitioning of Biomass-Burning Phenols and the Effects of Temperature and Salinity, Environ. Sci. Technol., 54, 3823–3830, 10.1021/acs.est.9b06443, 2020.

Tran, L. N., Abellar, K. A., Cope, J. D., and Nguyen, T. B.: Second-Order Kinetic Rate Coefficients for the Aqueous-Phase Sulfate Radical ($SO_4^{\bullet-}$) Oxidation of Some Atmospherically Relevant Organic Compounds, J. Phys. Chem. A, 126, 6517–6525, 10.1021/acs.jpca.2c04964, 2022.